Multi-objective Optimization of MWCNT Mixed Electric Discharge Machining of Al–30SiC$_p$ MMC Using Particle Swarm Optimization

Chander Prakash, Sunpreet Singh, Manjeet Singh, Parvesh Antil, Abdul Azeez Abdu Aliyu, A. M. Abdul-Rani and Sarabjeet S. Sidhu

Abstract In the present research work, the multi-walled carbon nanotube (MWCNT) mixed electric discharge machining of Al–SiC$_p$-based MMC has been proposed. The effect on MWCNT concentration, peak current, pulse duration, and duty cycle on the surface roughness and material removal rate has been investigated and multi-objective optimization of MWCNT mixed-EDM process parameters has been carried out for the machining of Al–30SiC$_p$ substrate using particle swarm optimization (PSO) technique. The SR and MRR increased with peak current and pulse duration in the case of EDM, but SR decreased and MRR increased with the dispersion of MWCNTs in EDM dielectric fluid. The empirical model has been developed by response surface methodology to interpret the relation between input parameters and output characteristics such as SR and MRR. However, the impacts of MWCNT mixed-EDM parameters on SR and MRR are clashing in nature; there is no single condition of machining parameters, which gives the best machining quality. Multi-objective particle swarm optimization technique was used to find the best optimal condition of MWCNT mixed-EDM parameters to minimize the SR and maximize the MRR. The best global solution where, maximum MRR (1.134 mm^3/min) and minimum SR (1.097 μm) obtained from the Pareto optimal front is at peak current = 15.59 A, pulse-on = 169.61 μs, duty cycle = 65.17%, and MWCNT powder concentration = 4.08 g/l. The MRR and SR are increased by 14.89 and 15.94%,

C. Prakash (✉) · S. Singh · M. Singh
School of Mechanical Engineering, Lovely Professional University, Phagwara 144411, Punjab, India
e-mail: chander.mechengg@gmail.com

P. Antil
Department of Mechanical Engineering, Northern India Engineering College, New Delhi, India

A. A. A. Aliyu · A. M. Abdul-Rani
Department of Mechanical Engineering, Institute of Technology Petronas Sdn. Bhd., Perak Tengah, Malaysia

S. S. Sidhu
Department of Mechanical Engineering, Beant College of Engineering & Technology, Gurdaspur 143521, Punjab, India

S. S. Sidhu et al. (eds.), *Futuristic Composites*, Materials Horizons: From Nature to Nanomaterials, https://doi.org/10.1007/978-981-13-2417-8_7

respectively, after mixing 4.08 g/l MWCNT concentration in dielectric fluid. From the above study, it is recommended for the process engineer to use the proposed optimal setting to achieve maximum MRR and minimum SR.

Keywords EDM · Al–SiC_p · MMC · SR · MRR · Nanofinishing
Process parameters · Optimization

1 Introduction

Al–SiC_p metal matrix composites (MMCs) have gained plentiful application in various industries, for instance, in automotive and aerospace sectors, owing to their one of a kind blend of mechanical properties, wear resistance, and retention of strength at elevated temperatures [1–5]. However, it has been witnessed that their full potential use is not escalating and hindered due to lack of machinability, with most of the conventional machining processes, often results into high tool wear, poor surface roughness, and high machining cost [6]. In this context, numerous researchers studied and investigated the suitability of advanced and nonconventional machining processes (such as electric discharge machining, abrasive jet machining, electron beam machining, and laser beam machining) to overcome the aforesaid bottlenecks [7, 8]. Among these, electric discharge machining (EDM) has been found as one of the best-suited machining technologies for machining Al–SiC_p MMC [9]. EDM is a thermomechanical process widely used to machine the hard and tough material with the ease [10]. The heat energy librated from the electrical sparks melts the workpiece surface and removed the material in the form of micron-size debris [11]. Prakash et al. reported the mechanism of material removal during EDM process in details, as illustrated in Fig. 1 [12]. In EDM, countless electrical sparks have been generated within fraction of seconds, which induced heat energy causing removal of material from workpiece surface [13]. In the presence of dielectric fluid, this librated heat energy thermally affected the top surface layer of workpiece material due to sudden quenching. Thus, various surface deformities like high surface roughness, high surface cracks, and micron size pits/dimples were shaped on the machined surface which breaks down the surface quality [14]. Keeping in mind the end objective to reduce the generation of surface flaws like micro-cracks, high ridges of re-disposition of molten pool, and high roughness, numerous modifications and progressions in EDM process has been carried out by numerous analysts [15, 16]. In the as-adopted modifications and progressions, the machining mechanisms of one or more process have been superimposed to take advantage of one process over other and called as hybridization. These hybridizations are such as electro-discharge diamond grinding (EDDG), ultrasonic vibration-assisted EDM (UVA-EDM), rotary-assisted EDM (RAEDM), HyFlex EDM, electro-discharge coating/surface modification by composite or green tool electrode, near dry EDM and powder mixed-EDM (PM-EDM) [17–25]. In comparison to all, the PM-EDM has been accepted and used as the most encouraging hybridized process to deal with reduction of surface defects and to enhance the sur-

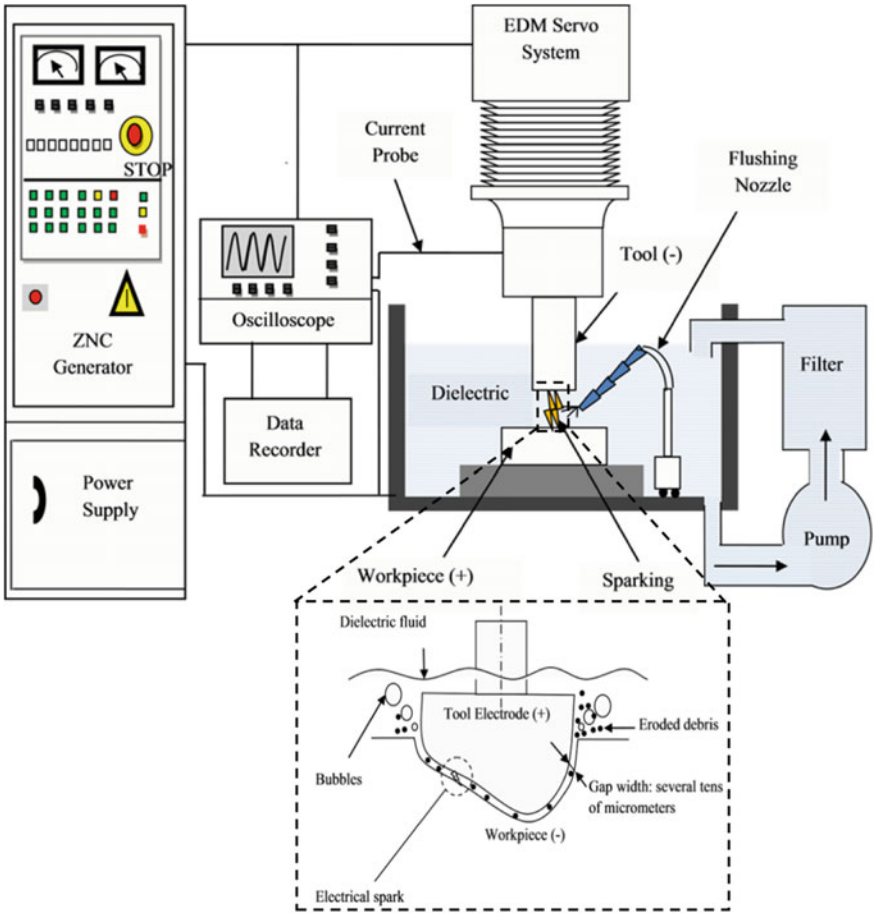

Fig. 1 Schematic illustrated the mechanism of material removal in EDM process [12]

face quality [26–30]. Prakash et al. [31] investigate the capability of PM-EDM not only to enhance the surface quality but also to improve the machining performance. It has been reported that with the dispersion of powder particles in the dielectric fluid, the uniformity and sparking area increased but the increased discharge gap which reduced the thermal energy resulted from the electrical sparks. As a result of this, small and tiny discharge craters were developed on the machined surface and lead to decrease in the SR value of the machined surface. On the other hand, with the dispersion of powder particles, the sparking area increased. As a consequence the top layer of workpiece is expelled in the form of micron debris from large locations; thus increased the MRR value.

Singh et al. studied the capability of PM-EDM to enhance the SR, MRR, and TWR characteristics by using tungsten powder particles as dielectric solvent [32–34]. It has been reported that tungsten powder in dielectric fluid enhanced the machining

gap and increased the machining contact area, as a result the material was removed in micron and sub-micron sized in large proportion with small pit size. Mohan et al. reported the application of PM-EDM for drilling the hole in Al–SiC MMCs and studied the effect of tool polarity along with other machining parameters on the machined hole surface quality [35]. Sidhu et al. investigated the efficacy of PM-EDM process to enhance the surface characteristics, machining performance, and surface properties of Al–SiC_p MMC and it has been reported that microhardness of the substrate surface was enhanced by the PM-EDM process using material migration method [36, 37]. Pecas and Henriques [38] reported the potential of PM-EDM for the finishing of workpiece material. Recently, Prakash et al. [39] explored the capability of PM-EDM as finishing process and studied the effect of surface finish achieved by PM-EDM process on the fatigue performance of Ti-based implant material. A number of researchers used PM-EDM process to enhance the machining performance, surface characteristics, and surface properties using micron-sized powder particles in the dielectric fluid [40–45]. The application of nonmetallic powder particles as a dielectric solvent has been used for the machining the work material with the aim of producing nanofinished part [46–48]. Miao et al. explored the capability of MWCNT mixedEDM process for the finishing of workpiece using miniature tool electrode. It was reported that with the use of MWCNT in EDM dielectric fluid, the machined surface quality and machining efficiency was improved by 70 and 66%, respectively [49]. Izman et al. [50] used the potential of MWCNT mixed-EDM for the reducing the recast layer thickness, improving the MRR and surface finish. It was reported that MRR and surface was improved by 7 and 9%, respectively. Prabhu and Vinayagam [51] reported that nanolevel surface finish ~75 nm was achieved on AISI-D2 steel substrate by MWCNT mixed-EDM process. Further, the utility of MWCNT-mixed-EDM for the finishing of Inconel 825 has been reported [52]. It was reported that surface finish of the components was enhanced by 34% than EDMed substrate. Sari et al. reported the nanofinishing of AISI H-13 tool by EDM using MWCNT mixed additive in dielectric fluid. The effect of MWCNT concentration on the re-deposition layer was studied and it was reported that the thickness of re-deposited layer was significantly. MWCNTs minimize the thickness of recast layer due to larger heat absorption [53]. When MWCNTs is added in to dielectric of EDM, produces 20% improvement in SR of AISI D2 tool steel [54]. Recently, Shabgard and Khosrozadeh [55] investigated the effect of MWCNT in dielectric fluid on SR, MRR, and TWR and it has been reported that the TWR and SR were significantly reduced by the use of MWCNT in dielectric fluid.

Optimization is very imperative to determine the best possible setting of input-process parameters to maximize the response characteristics. A number of single/conventional techniques such as Taguchi, response surface methodology, Grey relation have been adopted in the past to optimize the process parameters of EDM and PM-EDM process [56–61]. These techniques are only applicable for optimizing single parameter and are usually not favorable for multiparametric objectives, since outcomes get clashed. Non-dominated sorted genetic algorithm (NSGA)-II was found suitable for the multiobjective optimization of EDM and PM-EDM process parameters to maximize the machine efficiency and to obtain quality surface

[62, 63]. Padhee et al. [64] implemented the application of NSGA-II to determine the optimal setting of PM-EDM process parameters to maximize MRR and to minimize SR for EN-32 steel. Recently, Mohanty et al. [65] used the capability of particle swarm optimization (PSO) for the optimization of nano-Al_2O_3-mixed-EDM process parameters for maximizing MRR and minimizing SR and TWR. Kennedy and Eberhart presented PSO first time in 1995 as an effective transformative computational procedure to optimize the response characteristics [66]. The PSO is developed to solve the consistent nonlinear streamlining issues after identifying the behavior of natural swarm bird coming back to perch and observed in numerous types of winged creatures [67–69]. The PSO method can produce top notch arrangements inside short computation time and stable merging attributes [70–72]. Because of the great execution of the PSO system, numerous process engineers/scientists discover the PSO as a productive option over other inquiry calculations particularly when managing multi-target streamlining issues [73].

The surface quality and the machining performance of Al–30SiCp MMC is a challenging issue in the machining process. However, there is no study available on the machining of Al–30SiCp MMC using MWCNT-mixed-EDM. In this way, the current study investigated the effect of MWCNT concentration on SR and MRR, further more multiobjective particle swarm optimization has been carried out to determine the optimal best setting to maximize the MRR and minimize SR. Till date no research study is available, which considered implication of PSO for multiobjective optimization of NPM-EDM process for Al-30SiCp MMC by using CNTs as powder additive.

2 Experimental Planning and Optimization

2.1 Materials and Experimentation

Widely used Al–305SiC_p MMC was used as workpiece for machining using powder mixed electric discharge machining process. The surface of Al–305SiC_p MMC was well grounded and cleaned with ethanol followed by drying at room temperature. The machining of Al–30SiC_p workpiece was carried out by using multi-walled carbon nanotube (MWCNT) mixed-EDM process. The MWCNTS powder particles were used as dielectric solvent and mixed in dielectric fluid. The SEM micrograph of MWCNT powder particles are shown in Fig. 2. The experimental setup for the surface modification was in-house developed and called as nanopowder-mixed electric discharge machining (NPM-EDM), as shown in Fig. 3. In order to perform a NPM-EDM process, a separate tank of the dielectric capacity of 5 L was designed and MWCNT powder was mixed in the dielectric fluid at various concentrations 0, 2, 4, 6, 8 g/l. The die-sinking EDM machine (ELECTRONICA model 5535) has been utilized to conduct the experiments. A circular shape copper alloy rod of size ϕ

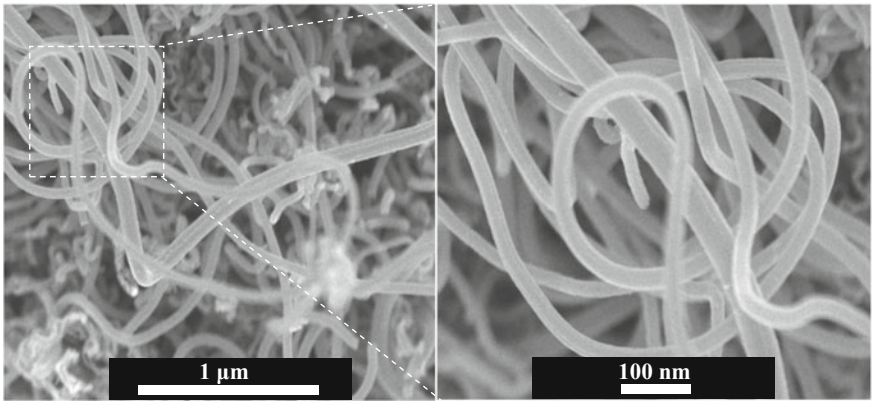

Fig. 2 SEM micrograph showing the morphology and size of MWCNT particles

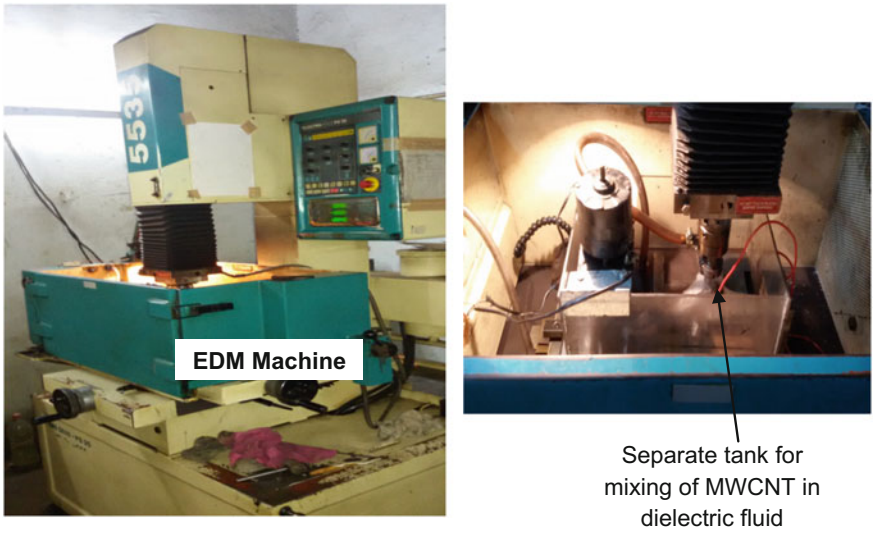

Fig. 3 Experimental setup of HA mixed electric discharge machining process

10 × 50 mm was used as an electrode for the machining process. Table 1 shows the detailed experimental conditions for the NPM-EDM process. From the initial trials, four input-process parameters were chosen for the examination. Table 1 presents the process parameters and their level.

Table 1 Process parameters and their levels

Working parameters	Description and levels
Tool electrode	Copper
Workpiece	Al–30SiC$_p$
Polarity	Tool (+), Workpiece (−)
Pulse current (A)	5 10 15 20 25
Pulse duration (μs)	50 100 150 200 250
Duty cycle (%)	8 24 40 56 80
MWCNT powder concentration (g/l)	0 2 4 6 8

2.2 Materials Characterization

The surface roughness (SR) and material removal rate (MRR) are considered as output response characteristics. The surface roughness was measured by Mitutoyo surface roughness tester. The MRR was computed by dividing the material removal per unit time, as per the procedure adopted previously [32]. In experimentation, central composite rotatable design (CCRD) has been used as a module of response surface methodology. Table 2 shows the design of experiment and obtained value of MRR and SR.

2.3 Optimization Using MO-PSO

Because of clashing nature of output characteristics as MRR and SR, the single optimal settings of process parameter is not fulfilling the goals. In such circumstances, MO-PSO gives better execution when contrasted with the customary improvement strategy because of their heartiness, independency of slope data, and utilization of inborn parallelism in looking through the plan space. The algorithm flowchart of MO-PSO algorithm is shown in Fig. 4.

3 Results and Discussions

3.1 Effect of Process Parameter on MRR and SR

Figure 5 shows the 3D response surface plot for the material removal rate (MRR) with respect to process parameters. Figure 5a shows the effect of interaction of peak current (I_p) and pulse duration (T_{on}) on MRR. The MRR increased with peak current (I_p), this is because when I_p increased, a large amount of heat is liberated

Table 2 Experimental design with response characteristics values of MRR and SR

S. No.	I_p	T_{on}	T_{au}	P_c	MRR	SR
1	10	100	24	2	1.001	1.412
2	20	100	24	2	1.105	1.589
3	10	200	24	2	0.985	1.514
4	20	200	24	2	1.164	1.721
5	10	100	56	2	1.155	1.529
6	20	100	56	2	1.230	1.758
7	10	200	56	2	1.149	1.65
8	20	200	56	2	1.345	1.862
9	10	100	24	6	1.159	1.487
10	20	100	24	6	1.229	1.839
11	10	200	24	6	1.230	1.625
12	20	200	24	6	1.450	1.987
13	10	100	56	6	1.215	1.419
14	20	100	56	6	1.307	1.731
15	10	200	56	6	1.234	1.645
16	20	200	56	6	1.424	1.928
17	5	150	40	4	1.072	1.305
18	25	150	40	4	1.195	1.899
19	15	50	40	4	1.201	1.456
20	15	250	40	4	1.299	1.678
21	15	150	8	4	1.051	1.467
22	15	150	72	4	1.262	1.607
23	15	150	40	0	1.132	1.89
24	15	150	40	8	1.425	1.939
25	15	150	40	4	1.165	1.551
26	15	150	40	4	1.176	1.529
27	15	150	40	4	1.138	1.489
28	15	150	40	4	1.161	1.549
29	15	150	40	4	1.145	1.512
30	15	150	40	4	1.175	1.512

and sunk into the workpiece. As a consequence, the size and shape of pits/craters on the modified surface increases, which further increases the MRR. The MRR value increased from 1.05 to 1.28 mm^3/min when peak current increased from 5 to 25 A. The MRR value first decreased with the pulse duration but, after certain value of pulse duration (150 μs), it starts increasing and goes on. This is due to the fact that discharge energy is proportional to pulse duration, thus an increase in the later enlarged the depth and width of craters [21, 74]. The MRR value increased from 1.03 to 1.55 mm^3/min when pulse duration increased from 150 to 250 μs at peak current and duty cycle of 5 A and 8%, respectively. The highest MRR (1.55 mm^3/min) is achieved at high level of peak current and high level of pulse duration. Figure 5b

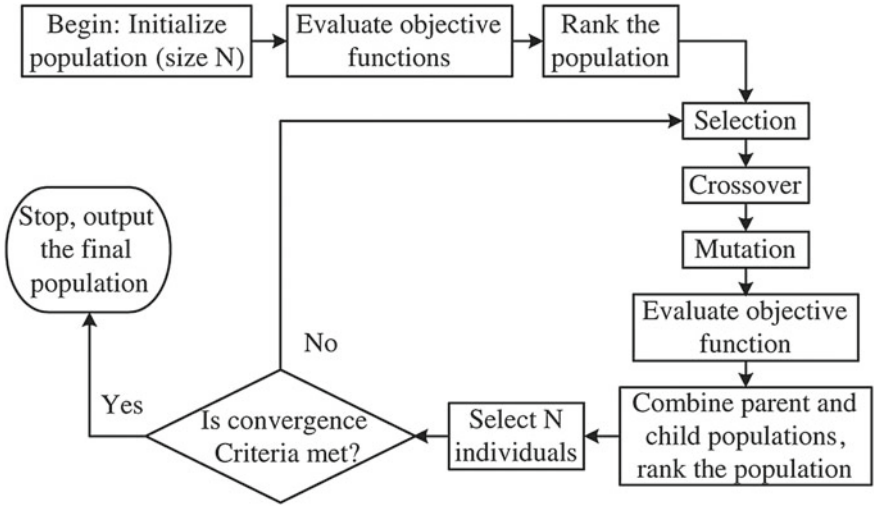

Fig. 4 Algorithm flowchart of MO-PSO

shows the effect of interaction of pulse duration (T_{on}) and powder concentration (P_c). The MRR increases with the MWCNT concentration in the dielectric fluid at any value of I_p and T_{on}. This is because, with the dispersion of MWCNT powder particles in the dielectric fluid, the spark locations increases and removed the material in larger proportion form the workpiece surface As a consequence, the top layer of workpiece is expelled in the form of micron-debris from large locations; thus, increased the MRR value. The MRR value increased from 1.15 to 1.38 mm^3/min, when MWCNT concentration increased from 0 to 6 g/l at pulse duration and duty cycle of 50 μs and 8%, respectively. The highest MRR (1.66 mm^3/min) is achieved at high level of peak current and high level of MWCNT concentration.

The MRR value is high in all cases of MWCNT mixed-EDM as compared to EDM. Figure 5c shows the variation of MRR value with respect to MWCNT concentration and duty factor. The MRR value increased with the duty factor at any value of peak current and pulse duration. This is due to the fact that as the duty cycle increases the pulse interval decreases and pulse duration increases. As a result, large amount of discharge energy sank into the workpiece material and causing removal of material in the form of deep and large craters. The MRR value increased from 0.90 to 1.35 mm^3/min, when duty cycle increased from 8 to 80% at peak current and pulse duration of 5 A and 50 μs, respectively. The highest MRR (1.35 mm^3/min) is achieved at high level of duty factor and high level of MWCNT concentration. The MRR increased very rapidly in combination with MWCNT concentration and pulse duration. The maximum MRR value has been obtained at high value of peak current, pulse duration, duty cycle, and MWCNT concentration. The best optimal condition where high MRR was obtained is $A3$, $B3$, $C3$, and $D3$. Table 3 presents the analysis of variance (ANOVA) for the MRR and showing all of the input-process parameters

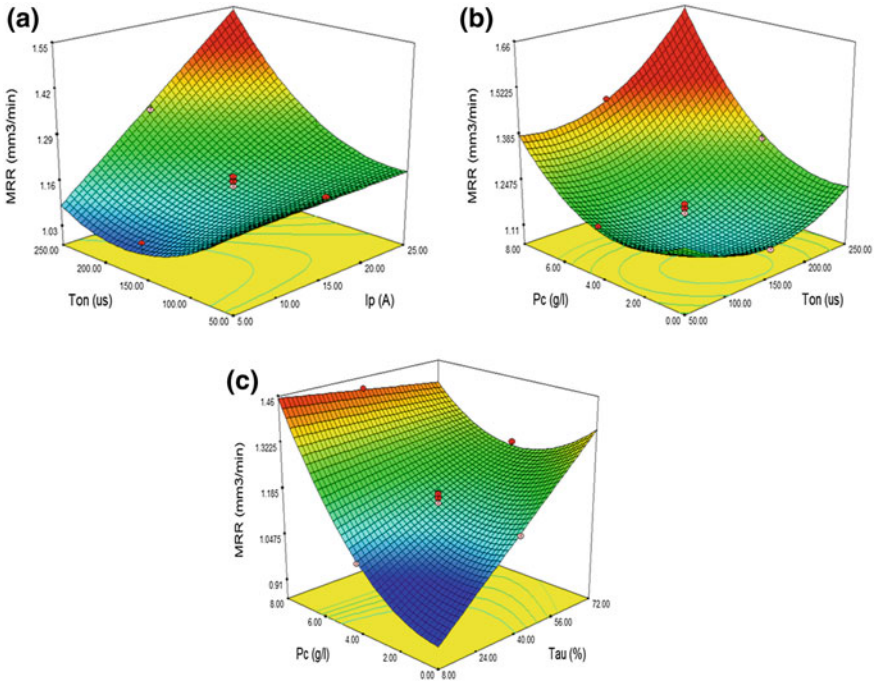

Fig. 5 3D response surface plot of MRR with respect to input-process parameters and their interaction

have significant contribution toward increasing the MRR. The mathematical model for the perdition of MRR was computed and represented in Eq. (3.1).

$$\begin{aligned}\text{MRR} = {} & 1.16243 - 5.27625\text{E}{-}003 * A - 4.62664\text{E}{-}003 * B \\ & + 7.01198\text{E}{-}003 * C - 0.013202 * D + 1.11325\text{E}{-}004 * A * B \\ & + 1.72313\text{E}{-}004 * B * D - 1.00059\text{E}{-}003 * C * D \\ & + 9.71031\text{E}{-}006 * B2 + 7.85020\text{E}{-}003 * D2 \end{aligned} \tag{3.1}$$

Figure 6 shows the 3D response surface plot for the surface roughness (SR) with respect to process parameters and their interactions. Figure 6a shows the effect of interaction of peak current (I_p) and pulse duration (T_{on}) on SR. As the peak current increases the SR increases, this is because when peak current increases, a large amount of heat is liberated and sunk into the workpiece. As a consequence, the increase in the size and shape of pits/craters increases the SR value from 1.22 to 1.80 μm. Similar trend was observed for the case of pulse duration parameter, as evidently. The SR value increases with the increase in pulse duration, because the discharge energy increased with the increase in pulse duration; thus deep and wide craters were developed on the machined surface. The SR value increased from 1.22

Table 3 ANOVA table for MRR

Source	Sum of squares	df	Mean square	F value	p-value (prob > F)
Model	0.353	9	0.0392	48.836	<0.0001 (significant)
I_p	0.078	1	0.0782	97.351	<0.0001
T_{on}	0.025	1	0.0250	31.097	<0.0001
T_{au}	0.055	1	0.0556	69.206	<0.0001
P_c	0.120	1	0.1204	149.799	<0.0001
$I_p * T_{on}$	0.012	1	0.0123	15.411	0.0008
$T_{on} * T_{au}$	0.004	1	0.0047	5.907	0.0246
$T_{au} * P_c$	0.016	1	0.0164	20.398	0.0002
T_{on}^2	0.017	1	0.0167	20.845	0.0002
P_c^2	0.028	1	0.0280	34.877	<0.0001
Residual	0.016	20	0.0008		
Lack of fit	0.014866711	15	0.0009	4.075	0.0643 (not significant)
Pure error	0.001216	5	0.0002		
Cor. total	0.369522252	29			
Std. dev. = 0.028357					R-squared = 0.956477
Mean = 1.19936					Adj R-squared = 0.936892
C.V. % = 2.364368					Pred R-squared = 0.901096
PRESS = 0.036547					Adeq Precision = 27.01855

to 1.50 μm when pulse duration increased from 50 to 250 μs. The lowest value of SR (1.22 μm) is obtained at low level of peak current and pulse duration.

Figure 6b shows the effect of interaction of MWCNT concentration (P_c) and pulse duration (T_{on}) on SR at any value of I_p and T_{on}. The SR value first decreases with MWCNT powder concentration but it starts increasing when the MWCNT powder concentration increases beyond 4 g/l. By the dispersion of MWCNT powder particles in the deionised water, the uniformity and sparking area increased but the increased discharge gap reduced the thermal energy resulted from the electrical sparks. As a result of this, small and tiny discharge craters were developed on the machined surface and lead to a decrease in the SR value of the machined surface [21]. The MWCNT powder concentration increased beyond 4 g/l, the powder particle get stuck with the plasma and get deposited on the machined surface. The SR value decreased from 1.79

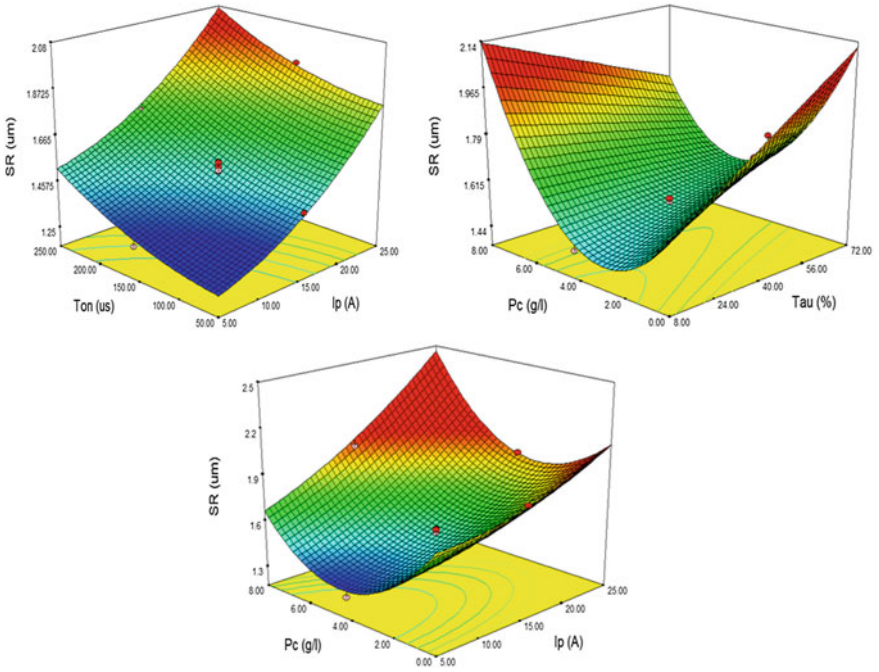

Fig. 6 3D response surface plot of SR with respect to input-process parameters and their interaction

to 1.35 μm, when MWCNT powder concentration increased from 0 to 4 g/l and it start increases from 1.35 to 2.14 μm when powder concentration increased from 6 to 8 g/l. The SR value increased with respect with the increase in duty cycle, due to the fact that as the duty cycle increased the pulse interval decreased and pulse duration increased. As a result, large amount of discharge energy sinked into the workpiece material and causing removal of material in the form of deep and large craters. The SR value increased from 1.79 to 2.12 μm, when duty cycle increased from 8 to 72%. The SR decreased very rapidly in combination with low peak current and 4 g/l MWCNT powder concentration. The minimum SR value was obtained at low value of peak current, pulse duration, duty cycle, and high level of MWCNT concentration. The best optimal condition where low SR was obtained is $A1$, $B1$, $C1$, and $D3$. Table 4 presents the analysis of variance (ANOVA) for the SR and showing all input-process parameters has significant contribution toward the SR. The mathematical model for the perdition of SR is computed, as represented in Eq. (3.2).

$$\begin{aligned} \mathrm{SR} = {} & 1.30396 - 7.79792\mathrm{E}{-}003 * A + 1.34333\mathrm{E}{-}003 * B \\ & + 7.71354\mathrm{E}{-}003 * C - 0.16473 * D + 3.02500\mathrm{E}{-}003 * A * D \\ & - 1.51953\mathrm{E}{-}003 * C * D + 7.79375\mathrm{E}{-}004 * A2 + 0.024402 * D2 \end{aligned} \quad (3.2)$$

Table 4 ANOVA table for SR

Source	Sum of squares	df	Mean square	F value	p-value (prob > F)
Model	0.931993779	8	0.116499	95.860887	<0.0001 (significant)
I_p	0.459820167	1	0.45982	378.36106	<0.0001
T_{on}	0.108272667	1	0.108273	89.091701	<0.0001
T_{au}	0.016432667	1	0.016433	13.521549	0.0014
P_c	0.021840667	1	0.021841	17.971499	0.0004
$I_p * P_c$	0.014641	1	0.014641	12.047284	0.0023
$T_{au} * P_c$	0.03783025	1	0.03783	31.128459	<0.0001
T_{on}^2	0.010798674	1	0.010799	8.8856424	0.0071
P_c^2	0.271007007	1	0.271007	222.99696	<0.0001
Residual	0.025521188	21	0.001215		
Lack of fit	0.022629854	16	0.001414	2.4458714	0.1643 (not significant)
Pure error	0.002891333	5	0.000578		
Cor. total	0.957514967	29			
Std. dev. = 0.035					R-squared = 0.9733
Mean = 1.64					Adj R-squared=0.9632
C.V. % = 2.13					Pred R-squared=0.9328
PRESS = 0.064					Adeq precision = 34.024

3.2 Multiobjective Optimization Using MO-PSO

It is noticed that when SR reduced, the MRR reduces. The MRR requires to be maximized while regulating the SR. Because of clashing nature of MRR and SR, it is important to locate the optimal set of conditions of input-process parameters that yield high MRR and least SR. Accordingly, the function MRR is changed over into minimization type and the objective functions are altered as below:

Objective 1 = Minimize (1/MRR);
Objective 2 = Minimize (SR).

With a specific end goal to perform such multiobjective optimization, a source code of the proposed algorithm MO-PSO was executed utilizing MATLAB. Figure 7 shows the spread of Pareto front which contains the 100 optimal set of conditions where both functions were optimized. In this way, the choice of a result against

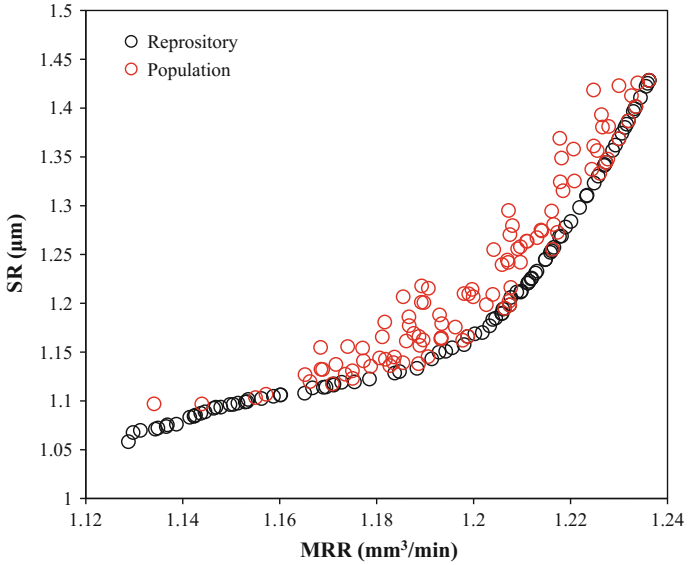

Fig. 7 Pareto optimal front of the MRR and SR using MO-PSO

Table 5 Optimal solutions obtained from MO-PSO with confirmation test

Solution No.	I_p (A)	T_{on} (µs)	τ (%)	P_c (g/l)	MRR (mm^3/min)	SR (µm)
1	25	250	80	0	1.23	1.428
2	15.59	169.61	65.17	4.08	1.13	1.097
3	24.27	242.75	77.08	0	1.23	1.423
4	21.85	221.51	68.19	2.43	1.17	1.14
5	19.24	199.86	72.30	2.41	1.16	1.13

different relies on item necessity as well as decision of process designer/engineer. It has been observed that MO-PSO predicted the best results within boundaries. Out of 100 global best solutions, the first 5 solutions are presented in Table 5.

3.2.1 Comparison of Experimental and Optimal MRR

In the investigation and comparing of experiential results of MRR with Pareto front, it is observed that the maximum MRR is 1.45 mm^3/min at peak current = 20 A, pulse-on = 200 µs, duty cycle = 24%, and MWCNT powder concentration = 6 g/l, corresponding to experiment no. 24 in Table 2. On the other hand, the maximum MRR obtained from the Pareto optimal front is 1.23 mm^3/min at peak current = 25 A, pulse-on = 250 µs, duty cycle = 80%, and MWCNT powder concentration = 0 g/l as shown in Table 2 (serial no. 1). The MRR predicted obtained from the optimal solution is

slightly lower than the experimental value. Moreover, from the 3D response of MRR (Fig. 5), it can be clearly seen that the MRR decreases if the pulse duration and duty cycle increases. So, it indicates that proper selection of process parameter level gives the maximum MRR. From Table 2 (experimental results no. 1), the minimum MRR is 0.987 mm^3/min at peak current = 20 A, pulse-on = 200 μs, duty cycle = 24%, and MWCNT powder concentration = 6 g/l. On the other hand, the minimum MRR obtained from the Pareto optimal front is 1.134 mm^3/min at peak current = 15.59 A, pulse-on = 169.61 μs, duty cycle = 65.17%, and MWCNT powder concentration = 4.08 g/l. The results show that the lower MRR obtained from optimal solution is much higher (about more than 1.7 times) as compared to the experimental value. This is because the MRR increases with increase of MWCNT powder concentration as more stable spark is generated in the machining zone.

3.2.2 Comparison of Experimental and Optimal SR

In the investigation and comparing of experiential results of SR with Pareto front, it is observed that the maximum SR is 1.987 μm at peak current = 20 A, pulse-on = 200 μs, duty cycle = 24%, and MWCNT powder concentration = 6 g/l corresponding to experiment no. 12 in Table 2. On the other hand, the maximum SR obtained from the Pareto optimal front is 1.4285 μm at peak current = 25 A, pulse-on = 250 μs, duty cycle = 80%, and MWCNT powder concentration = 0 g/l corresponding as shown in Table 2 (serial no. 1). The predicted SR value obtained from the optimal solution is very much lower than the experimental. Moreover, from the 3D response of SR (Fig. 6), it can be clearly seen that the SR decreases if the pulse duration decreases. So, it indicates that proper selection of process parameter level gives the maximum SR. From the Table 2 (experimental results no. 17), the minimum SR is 1.305 μm at peak current = 5 A, pulse-on = 150 μs, duty cycle = 40%, and MWCNT powder concentration = 4 g/l corresponding. On the other hand, the minimum SR obtained from the Pareto optimal front is 1.097 μm at peak current = 15.59 A, pulse-on = 169.61 μs, duty cycle = 65.17%, and MWCNT powder concentration = 4.08 g/l corresponding. The results show that the lower SR obtained from optimal solution is much higher (about more than 2.66 times) as compared to the experimental value. This is because the SR decreases with increase of MWCNT powder concentration as more stable spark is generated in the machining zone.

4 Conclusions

In this chapter, particle swarm optimization (PSO) is used for the multi-objective optimization of process parameters of MWCNT mixed-EDM process. The following conclusions are drawn after the critical observation of the results obtained:

1. The MRR increases with peak current, pulse duration, duty factor, and MWCNT powder concentration. The addition of MWCNT in dielectric fluid increases the uniformity and spark locations, as a result, more materials is removed from workpiece surface in comparison to EDM only.
2. The SR increases with peak current, pulse duration, and duty factor. It decreases with increase of MWCNT powder concentration, but, after 4 g/l, it starts increasing. The addition of MWCNT in dielectric fluid increases the discharge gap; as a result the reduced level of thermal energy caused the formation of micron and sub-micron debris, thereby improved the surface finish.
3. The MO-PSO provides a number of combinations of process parameters in comparison to experimental values, which indicates that proper selection of process parameters enhances machining efficiency.
4. The combinations of high peak current, pulse duration, duty factor, powder concentration are more suitable for getting higher value of MRR.
5. The combination of low peak current, moderate pulse duration, high duty factor, and 2–4 g/l MWCNT powder concentration are more suitable for the better surface finish.
6. The MO-PSO provides set of optimal solutions as presented in Pareto front. The optimum solutions facilitate for process engineer to select the optimal value of control parameters depending upon product requirement.

References

1. Buschmann R (2006) Preforms for the reinforcement of light metals—manufacture, applications and potential. In: Kainer KU (ed) Metal matrix composites: custom-made materials for automotive and aerospace engineering. Wiley-VCH Verlag GmbH & Co. KGaA, Weinheim, pp 77–94
2. Pai BC, Pillai RM, Satyanarayana KG (1998) Light metal matrix composites—present status and future strategies. NML, Jamshedpur, pp 26–40
3. Antil P, Singh S, Manna A (2017) Glass fibers/SiC_p reinforced epoxy composites: effect of environmental conditions. J Compos Mater 52(9):1253–1264
4. Antil P, Singh S, Manna A (2018) Effect of reinforced SiC particulates of different grit size on mechanical and tribological properties of hybrid PMCs. Mater Today Proc 5(2):8073–8079
5. Antil P, Singh S, Manna A (2018) Analysis on effect of electroless coated SiC_p on mechanical properties of polymer matrix composites. Part Sci Technol. https://doi.org/10.1080/02726351.2018.1444691 (In press)
6. Weinert K, Lange M, Petzoldt V (2002) Machining of metal matrix composites. In: Proceedings of ESDA2002: 6th Biennial conference on engineering systems, design and analysis, Istanbul, Turkey, 8–11 July 2002. ASME, New York
7. Muthuramalingam T, Mohan B (2015) A review on influence of electrical process parameters in EDM process. Arch Civil Mech Eng 15:87–94
8. Antil P, Singh S, Manna A (2017) Electrochemical discharge drilling of sic reinforced polymer matrix composite using Taguchi's grey relational analysis. Arab J Sci Eng 43(3):1257–1266
9. Muller F, Monaghan J (2000) Non-conventional machining of particle reinforced metal matrix composite. Int J Mach Tools Manuf 40(9):1351–1366
10. Rajurkar KP (1994) Nontraditional manufacturing processes (Chap. 13). In: Handbook of design manufacturing and automation. Wiley, USA

11. Abbas NM, Solomon DG, Bahari MF (2007) A review on current research trends in electrical discharge machining (EDM). Int J Mach Tools Manuf 47:1214–1228
12. Prakash C, Kansal HK, Pabla BS, Puri S, Aggarwal A (2016) Electric discharge machining a potential choice for surface modification of metallic implants for orthopedics applications: a review. Proc Inst Mech Eng Part B J Eng Manuf 230(2):331–353. https://doi.org/10.1177/0954405415579113
13. Prakash C, Kansal HK, Pabla BS, Puri S (2015) Processing and characterization of novel biomimetic nanoporous bioceramic surface on β-Ti implant by powder mixed electric discharge machining. J Mater Eng Perform 24:3622–3633. https://doi.org/10.1007/s11665-015-1619-6
14. Prakash C, Uddin MS (2017) Surface modification of β-phase Ti implant by hydroxyapatite mixed electric discharge machining to enhance the corrosion resistance and in-vitro bioactivity. Surf Coat Technol 236(Part A):134–145. https://doi.org/10.1016/j.surfcoat.2017.07.040
15. Kumar S, Singh R, Singh TP, Sethi BL (2009) Surface modification by electrical discharge machining: a review. J Mater Process Technol 209:3675–3687
16. Garg RK, Singh KK, Sachdeva A, Sharma VS, Ojha K, Singh S (2010) Review of research work in sinking EDM and WEDM on metal matrix composite materials. Int J Adv Manuf Technol 50:611–624
17. Agrawal SS, Yadava V (2016) Development and experimental study of surface-electrical discharge diamond grinding of Al–10 wt%SiC composite. J Inst Eng India Ser C 97:1. https://doi.org/10.1007/s40032-015-0183-z
18. Shabgard MR, Alenabi H (2015) Ultrasonic assisted electrical discharge machining of Ti–6Al–4V alloy. Mater Manuf Process 30(8):991–1000. https://doi.org/10.1080/10426914.2015.1004686
19. Dwivedi AP, Choudhury SK (2016) Effect of tool rotation on MRR, TWR and surface integrity of AISI-D3 steel using rotary EDM process. Mater Manuf Process. https://doi.org/10.1080/10426914.2016.1140198
20. Pirani C, Iacono F, Generali L, Sassatelli P, Nucci C, Lusvarghi L, Gandolfi MG, Prati C (2015) HyFlex EDM: superficial features, metallurgical analysis and fatigue resistance of innovative electro discharge machined NiTi rotary instruments. Int Endod J. https://doi.org/10.1111/iej.12470
21. Krishna ME, Patowari PK (2014) Parametric study of electric discharge coating using powder metallurgical green compact electrodes. Mater Manuf Process 29(9):1131–1138. https://doi.org/10.1080/10426914.2014.930887
22. Muthuramalingam T, Mohan B, Jothilingam A (2014) Effect of tool electrode resolidification on surface hardness in electrical discharge machining. Mater Manuf Process 29(11–12):1374–1380
23. Gill AS, Kumar S (2016) Surface roughness and microhardness evaluation for EDM with Cu–Mn powder metallurgy tool. Mater Manuf Processes 31(4):514–521. https://doi.org/10.1080/10426914.2015.1070412
24. Shen Y, Liu Y, Zhang Y, Dong H, Sun P, Wang X, Zheng C, Ji R (2016) Effects of an electrode material on a novel compound machining of Inconel 718. Mater Manuf Process 31(7):845–851. https://doi.org/10.1080/10426914.2015.1019133
25. Ahmed A (2016) Deposition and analysis of composite coating on aluminum using Ti–B4C powder metallurgy tools in EDM. Mater Manuf Process 31(6):467–474. https://doi.org/10.1080/10426914.2015.1025967
26. Pecas P, Henriques E (2008) Effect of the powder concentration and dielectric flow in the surface morphology in electrical discharge machining with powder-mixed dielectric (PMD-EDM). Int J Adv Manuf Technol 37:1120–1132
27. Pecas P, Henriques E (2008) Electrical discharge machining using simple and powder mixed dielectric: the effect of the electrode area on the surface roughness and topography. J Mater Process Technol 200:250–258
28. Prakash C, Kansal HK, Pabla BS, Puri S (2015) Potential of powder mixed electric discharge machining to enhance the wear and tribological performance of β-Ti implant for orthopedic applications. J Nanoeng Nanomanuf 5(4):261–269. https://doi.org/10.1166/jnan.2015.1245

29. Prakash C, Kansal HK, Pabla BS, Puri S (2016) Multi-objective optimization of powder mixed electric discharge machining parameters for fabrication of biocompatible layer on β-Ti alloy using NSGA-II coupled with Taguchi based response surface methodology. J Mech Sci Technol 30(9):4195–4204. https://doi.org/10.1007/s12206-016-0831-0
30. Prakash C, Kansal HK, Pabla BS, Puri S (2016) Effect of surface nano-porosities fabricated by powder mixed electric discharge machining on bone-implant interface: an experimental and finite element study. Nanosci Nanotechnol Lett 8(10):815–826. https://doi.org/10.1166/nnl.2016.2255
31. Prakash C, Kansal HK, Pabla BS, Puri S (2017) Experimental investigations in powder mixed electrical discharge machining of Ti–35Nb–7Ta–5Zr β–Ti alloy. Mater Manuf Process 32(3):274–285. https://doi.org/10.1080/10426914.2016.1198018
32. Singh B, Kumar J, Kumar S (2016) Investigation of the tool wear rate in tungsten powder-mixed electric discharge machining of AA6061/10%SiCp composite. Mater Manuf Process 31(4)
33. Singh B, Kumar J, Kumar S (2015) Influences of process parameters on MRR improvement in simple and powder-mixed EDM of AA6061/10%SiC composite. Mater Manuf Process 30(3)
34. Singh B, Kumar J, Kumar S (2014) Experimental investigation on surface characteristics in powder-mixed electrodischarge machining of AA6061/10%SiC composite. Mater Manuf Process 29(3)
35. Mohan B, Rajadurai A, Satyanarayana KG (2002) Effect of SiC and rotation of electrode on electric discharge machining of Al-SiC composite. J Mater Process Technol 124:297–304
36. Sidhu SS, Batish A, Kumar S (2013) Neural network-based modeling to predict residual stresses during electric discharge machining of Al/SiC metal matrix composites. Proc Inst Mech Eng Part B J Eng Manuf 227(11), 1679–1692
37. Sidhu SS, Batish A, Kumar S (2014) Study of surface properties in particulate-reinforced metal matrix composites (MMCs) using powder-mixed electrical discharge machining (EDM). Mater Manuf Process 29(1)
38. Pecas P, Henriques E (2003) Influence of silicon powder-mixed dielectric on conventional electrical discharge machining. Int J Mach Tools Manuf 43(14):1465–1471
39. Prakash C, Kansal HK, Pabla BS, Puri S (2015) Powder mixed electric discharge machining an innovative surface modification technique to enhance fatigue performance and bioactivity of β-Ti implant for orthopaedics application. J Comput Inf Sci Eng 14(4):1–9. https://doi.org/10.1115/1.4033901
40. Talla G, Gangopadhayay S, Biswas CK (2017) State of the art in powder-mixed electric discharge machining: a review. Proc Inst Mech Eng Part B J Eng Manuf 231(14):2511–2526
41. Ojha K, Garg RK, Singh KK (2011) Parametric optimization of PMEDM process using chromium powder mixed dielectric and triangular shape electrodes. J Miner Mater Charact Eng 10(11):1087–1102
42. Singh S, Yeh MF (2012) Optimization of abrasive powder mixed EDM of aluminum matrix composites with multiple responses using gray relational analysis. J Mater Eng Perform 21(4):481–491
43. Kumar S, Singh R, Singh TP, Sethi BL (2009) Comparison of material transfer in electrical discharge machining of AISI H13 die steel. J Mech Eng Sci 223(7):1733–1740
44. Kumar S, Batra U (2012) Surface modification of die steel materials by EDM method using tungsten powder mixed dielectric. J Manuf Process 14:35–40
45. Hu FQ, Cao FY, Song BY, Hou PJ, Zhang Y, Chen K, Wei JQ (2013) Surface properties of SiCp/Al composite by powder-mixed EDM. Procedia CIRP 6:101–106
46. Jahan MP, Rahman M, Wong YS (2011) Study on the nano-powder-mixed sinking and milling micro-EDM of WC-Co. Int J Adv Manuf Technol 53:167–180
47. Prihandana GS, Mahardika M, Hamdi M, Wong YS, Mitsui K (2011) Accuracy improvement in nanographite powder-suspended dielectric fluid for micro-electrical discharge machining processes. Int J Adv Manuf Technol 56:143–149
48. Baseri H, Sadeghian S (2016) Effects of nanopowder TiO_2-mixed dielectric and rotary tool on EDM. Int J Adv Manuf Technol 83(1–4):519–528

49. Mai C, Hocheng H, Huang S (2012) Advantages of carbon nano tubes in electrical discharge machining. Int J Adv Manuf Technol 59(1–4):111–117
50. Izman S, GHodsiyeh D, Hamed T, Rosliza R, Rezazadeh M (2012) Effects of adding multiwalled carbon nanotube into dielectric when EDMing titanium alloy. Adv Mater Res 463–464:1445–1449
51. Prabhu S, Vinayagam BK (2010) Analysis of surface characteristics of AISI D2 tool steel material using EDM process with Single wall carbon nano tubes. Int J Eng Technol 2(1):35–41
52. Prabhu S, Vinayagam BK (2012) Modeling the machining parameters of AISI D2 tool steel material with multi wall carbon nano tube in electrical discharge machining process using response surface methodology. Int J Phys Sci 7(2):297–305
53. Prabhu S, Vinayagam BK (2009) Effect of graphite electrode material on EDM of AISI D2 tool steel with multiwall Carbon Nanotube using regression analysis. Int J Eng Stud 1(2):93–104
54. Sari MM, Noordin MY, Brusa S (2013) Role of multi-wall carbon nanotubes on the main parameters of the electrical discharge machining (EDM) process. Int J Adv Manuf Technol 68(5–8):1095–1102
55. Shabgard M, Khosrozadeh B (2017) Investigation of carbon nanotube added dielectric on the surface characteristics and machining performance of Ti–6Al–4V alloy in EDM process. J Manuf Process 25:212–219
56. Ikram A, Mufti NA, Saleem MQ, Khan AR (2013) Parametric optimization for surface roughness, kerf and MRR in wire electrical discharge machining (WEDM) using Taguchi design of experiment. J Mech Sci Technol 27(7):2133–2141
57. Dao TP, Huang SC (2015) Robust design for a flexible bearing with 1-DOF translation using the Taguchi method and the utility concept. J Mech Sci Technol 29(8):3309–3320
58. Jung JH, Kwon WT (2010) Optimization of EDM process for multiple performance characteristics using Taguchi method and Grey relational analysis. J Mech Sci Technol 24(5):1083–1090
59. Santhanakumar M, Adalarasan R, Rajmohan M (2016) Parameter design for cut surface characteristics in abrasive waterjet cutting of Al/SiC/Al_2O_3 composite using grey theory based RSM. J Mech Sci Technol 30(1):371–379
60. Gopalakannan S, Senthilvelan T (2014) Optimization of machining parameters for EDM operations based on central composite design and desirability approach. J Mech Sci Technol 28(3):1045–1053
61. Tao Z, Yaoyao S, Xiaojun L, Tianran H (2016) Optimization of abrasive flow polishing process parameters for static blade ring based on response surface methodology. J Mech Sci Technol 30(3):1085–1093
62. Yadav RN, Yadava V, Singh GK (2014) Application of non-dominated sorting genetic algorithm for multi-objective optimization of electrical discharge diamond face grinding process. J Mech Sci Technol 28(6):2299–2306
63. Bharti PS, Maheshwari S, Sharma C (2012) Multi-objective optimization of electric-discharge machining process using controlled elitist NSGA-II. J Mech Sci Technol 26(6):1875–1883
64. Padhee S, Nayak N, Panda SK, Dhal PR, Mahapatra SS (2012) Multi-objective parametric optimization of powder mixed electro-discharge machining using response surface methodology and non-dominated sorting genetic algorithm. Sadhana 37(2):223–240
65. Mohanty S, Mishra A, Nanda BK, Routara BC (2017) Multi-objective parametric optimization of nano powder mixed electrical discharge machining of AlSiCp using response surface methodology and particle swarm optimization. Alexandria Eng J
66. Kennedy J, Eberhart R (1995) Particle swarm optimization. In: Proceedings of the IEEE international conference on neural networks, vol 4, pp 1942–1948. IEEE
67. Kalayci CB, Gupta SM (2013) A particle swarm optimization algorithm with neighborhood-based mutation for sequence dependent disassembly line balancing problem. Int J Adv Manuf Technol 69(1–4):197–209
68. Jia Q, Seo Y (2013) An improved particle swarm optimization for the resource-constrained project scheduling problem. Int J Adv Manuf Technol 67(9–12):2627–2638
69. Li X, Gao L, Wen X (2012) Application of an efficient modified particle swarm optimization algorithm for process planning. Int J Adv Manuf Technol 67(5–8):1355–1369

70. Yildiz AR, Solanki KN (2012) Multi-objective optimization of vehicle crashworthiness using a new particle swarm based approach. Int J Adv Manuf Technol 59(1–4):367–376
71. Yang WA, Guo Y, Liao WH (2011) Optimization of multi-pass face milling using a fuzzy particle swarm optimization algorithm. Int J Adv Manuf Technol 54(1–4):45–57
72. Costa A, Celano G, Fichera S (2011) Optimization of multi-pass turning economies through a hybrid particle swarm optimization technique. Int J Adv Manuf Technol 53(5–8):421–433
73. Srinivas J, Giri R, Yang SH (2009) Optimization of multi-pass turning using particle swarm intelligence. Int J Adv Manuf Technol 40(1–2):56–66
74. Aliyu AAA, Abdul-Rani AM, Ginta TL, Prakash C, Axinte E, Razak MA, Ali S (2017) A review of additive mixed-electric discharge machining: current status and future perspectives for surface modification of biomedical implants. Adv Mater Sci Eng